J|A|C|S
ARTICLES
Published on Web 08/08/2006

Single-Molecule Charge-Transport Measurements that Reveal Technique-Dependent Perturbations

Dwight S. Seferos,[†] Amy Szuchmacher Blum,[‡] James G. Kushmerick,*[,§] and Guillermo C. Bazan*[,†]

Departments of Chemistry & Biochemistry and Materials, Institute for Polymers and Organic Solids, University of California, Santa Barbara, California 93106, Naval Research Laboratory, Washington, D.C. 20375, and National Institute of Standards and Technology, Gaithersburg, Maryland 20899

Received May 3, 2006; E-mail: james.kushmerick@nist.gov; bazan@chem.ucsb.edu

Abstract: We compare scanning tunneling microscopy (STM) imaging with single-molecule conductive atomic force microscopy (C-AFM) measurements by probing a series of structurally related thiol-terminated oligo(phenylenevinylene)s (OPVs) designed to have unique charge-transport signatures. When one or two methylene spacers are inserted between the thiol points of attachment and the OPV core, a systematic reduction in the imaged molecular transconductance and the current transmitted through a metal−molecule−metal junction containing the molecule is observed, indicating good agreement between STM and C-AFM measurements. However, a structure where the OPV backbone is interrupted by a [2.2]paracyclophane core has a low molecular transconductance, as determined from STM images, and a high measured single-molecule conductance. This apparent disconnect can be understood by comparing the calculated molecular orbital topology of the OPV with one thiol bound to a gold surface (the geometry in the STM experiment) with the topology of the molecule with both thiol termini bound to gold (relevant to C-AFM). In the former case, a single contact splits low-lying molecular orbitals into two discrete fragments, and in the latter case, molecular orbitals that span the entire molecule are observed. Although the difference in observed conductance between the two different measurements is resolved, the overall set of observations highlights the importance of using combined techniques to better characterize charge-transport properties relevant to molecular electronics.

Introduction

The possibility of using individual organic molecules for molecular-scale electronic applications has prompted the development of numerous techniques to measure the charge-transport properties of a few or single molecules.[1] Transport measurements on a small collection of molecules can be accomplished by probing a self-assembled monolayer[2] (SAM) of the molecule of interest with a top contact such as a conducting atomic force microscope tip,[3] a mercury drop electrode,[4] or an evaporated metal.[5] The charge-transport properties of SAMs can also be measured in crossed-wire[6] or inline metallic nanowire[7] geometries or by bridging two closely spaced SAM-functionalized electrode surfaces with a metallic bead.[8] In addition to these ensemble measurements, a number of methods have been developed that contact and measure the charge transport of individual molecules. These techniques include mechanical break junctions[9] and scanning probe measurements, such as scanning tunneling microscopy[10] (STM) and conductive atomic force microscopy[11] (C-AFM).

The growing number of measurements, and differences between them, may prompt some critics to question how much information can be obtained by using a single method. Cross-correlation of techniques is important, not only to provide confidence in the measurements but also because it yields insight

[†] University of California.
[‡] Naval Research Laboratory.
[§] National Institute of Standards and Technology.

(1) Mantooth, B. A.; Weiss, P. S. *Proc. IEEE* **2003**, *91*, 1785−1802.
(2) Love, J. C.; Estroff, L. A.; Kriebel, J. K.; Nuzzo, R. G.; Whitesides, G. M. *Chem. Rev.* **2005**, *105*, 1103−1169.
(3) Wold, D. J.; Frisbie, C. D. *J. Am. Chem. Soc.* **2001**, *123*, 5549−5556.
(4) Holmlin, R. E.; Hagg, R.; Chabinyc, M. L.; Ismagilov, R. F.; Cohen, A. E.; Terfort, A.; Rampi, M. N.; Whitesides, G. M. *J. Am. Chem. Soc.* **2001**, *123*, 5075−5085.
(5) Chen, J.; Reed, M. A.; Rawlett, A. M.; Tour, J. M. *Science* **1999**, *286*, 1550−1552.
(6) Kushmerick, J. G.; Holt, D. B.; Pollack, S. K.; Ratner, M. A.; Yang, J. C.; Schull, T. L.; Narci, J.; Moore, M. H.; Shashidhar, R. *J. Am. Chem. Soc.* **2002**, *124*, 10654−10655.
(7) Cai, L. T.; Skulason, H.; Kushmerick, J. G.; Pollack, S. K.; Naciri, J.; Shashidhar, R.; Allara, D. L.; Mallouk, T. E.; Mayer, T. S. *J. Phys. Chem. B* **2004**, *108*, 2827−2832.
(8) (a) Amlnai, I.; Rawlett, A. M.; Nagahara, L. A.; Tsui, R. *Appl. Phys. Lett.* **2002**, *80*, 2761−2763. (b) Long, D. P.; Patterson, C. H.; Moore, M. H.; Seferos, D. S.; Bazan, G. C.; Kushmerick, J. G. *Appl. Phys. Lett.* **2005**, *86*, 153105.
(9) (a) Reed, M. A.; Zhou, C.; Muller, C. J.; Burgin, T. P.; Tour, J. M. *Science* **1997**, *278*, 252−254. (b) Mayor, M.; von Hanisch, C.; Weber, H. B.; Reichert, J.; Beckman, D. *Angew. Chem., Int. Ed.* **2002**, *41*, 1183−1186. (c) Xu, B.; Tao, N. J. *Science* **2003**, *301*, 1221−1224.
(10) (a) Bumm, L. A.; Arnold, J. J.; Cygan, M. T.; Dunbar, T. D.; Burgin, T. P.; Jones, L., II; Allara, D. L.; Tour, J. M.; Weiss, P. S. *Science* **1996**, *271*, 1705−1707. (b) Blum, A. S.; Kushmerick, J. G.; Pollack, S. K.; Yang, J. C.; Moore, M.; Naciri, J.; Shashidhar, R.; Ratna, B. R. *J. Phys. Chem. B* **2004**, *108*, 18124−18128.
(11) Cui, X. D.; Primak, A.; Zarate, X.; Torfohr, J.; Sankey, O. F.; Moore, A. L.; Moore, T. A.; Gust, D.; Harris, G.; Lindsay, S. M. *Science* **2001**, *294*, 571−574.

10.1021/ja062898j CCC: $33.50

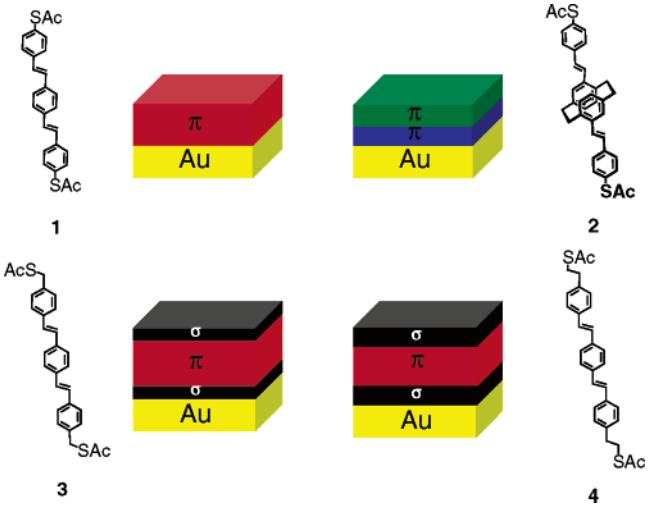

Figure 1. Structures of the molecules examined in this study and a representation of their films on a gold surface. In charge-transport measurements, the top of the film is contacted by a metallic probe (not shown).

into which effects arise from differences in contacts and/or geometries (dependent on the measurement test structure) and from inherent molecular properties.[12] Although it is conceptually simple to compare properties such as resistances obtained from current−voltage measurements by simply scaling for the number of molecules contacted in the measurement, the uncertainty in that number presents a problem. Additionally, comparing techniques that indirectly measure conductance, such as STM imaging, with direct molecular conductivity measurements is even less straightforward. STM offers the advantages of simultaneous imaging and measurement and also gives additional information about the local density of states of adsorbed molecules. STM measurements have been used to examine molecular switching[13] and to provide a measure of molecular transconductance[14] by giving an estimation of the tunneling decay constant. However, these data are at best an indirect measure of molecular transconductance and their correlation to molecular conductivity has not been directly investigated.

In this contribution, we compare the tunneling decay constant, determined from STM imaging, with metal−molecule−metal conductivity measurements, obtained from C-AFM measurements, for single molecules isolated in an alkane thiol matrix. We provide for these studies a series of structurally related distyrylbenzene derivatives that are expected to display unique charge-transport properties (Figure 1). For example, recent independent reports have shown that the incorporation of a methylene spacer into a conjugated molecule leads to both a reduced transconductance in STM measurements[14b] and a reduced conductivity in molecular junction measurements[15] when compared to their analogous fully delocalized structures. Conversely, results on a molecule that contains a [2.2]paracyclophane core demonstrate that this structural perturbation does not significantly reduce transport through the molecule when compared to its fully through-bond delocalized analogue.[16] Examination of these molecular structures provides a basis for cross-comparison of STM and C-AFM measurements and can be used to evaluate whether such a combined technique approach yields a better understanding of molecular charge-transport properties.

Results and Discussion

Molecular Design and Synthesis. As shown in Figure 1, the molecular fragments in this study are thioacetate-terminated oligomers of the phenylenevinylene (OPV) structural motif. The thioacetate group hydrolyzes during the assembly protocol to provide thiol functionalities for chemical attachment onto the gold surfaces. The first molecular structure is the fully π-conjugated OPV, 1,4-bis[4′-(acetylthio)styryl]benzene (**1**), which has thioacetate groups positioned directly on the OPV π-system. The second compound, 4,12-bis[4′-(acetylthio)styryl][2.2]-paracyclophane (**2**), is similar to **1** but has the phenylenevinylene structure interrupted by the [2.2]paracyclophane core. This arrangement represents a well-defined transannular extension of conjugation[17] and has been demonstrated to have a charge-transport efficiency similar to that for **1**.[16] The last two structures, 1,4-bis[4′-(thioacetylmethyl)styryl]benzene (**3**) and 1,4-bis[4′-(thioacetylethyl)styryl]benzene (**4**) are a progression of structure **1** through the systematic incorporation of one or two methylene spacer units between the π-conjugated OPV core and the thioacetate points of attachment.

Compounds **1** and **2** were synthesized by using our previously reported thioanisol precursor route.[18] The synthesis of these structures, which have their thiol anchor groups attached directly onto their aromatic core, involves masking the reactive arylthiol as an arylthiomethyl precursor. These precursors are tolerant of Wittig[19] and Heck-type[20] reactions for forming the C−C double bonds contained within the structures and can be converted to their thioacetate analogues by following a simple and high-yielding dealkylation step.[21] Additionally, this step isomerizes the π-backbone to the *all-E* isomers, regardless of the starting material stereochemistry.[18]

The synthesis of **3**, a distyrylbenzene with methylthioacetate end groups, begins with the conversion of 4-bromomethylbenzonitrile to 4-bromomethylbenzaldehyde in 71% yield by DIBAL reduction (Scheme 1).[22] Next, the 2-fold Wittig coupling of 4-bromomethylbenzaldehyde and 1,4-bis(methyltriphenyl-

(12) (a) Selzer, Y.; Cai, L.; Cabassi, M. A.; Yao, Y.; Tour, J. M.; Mayer, T. S.; Allara, D. L. *Nano Lett.* **2005**, *5*, 61−65. (b) Blum, A. S.; Kushmerick, J. G.; Long, D. P.; Patterson, C. H.; Yang, J. C.; Henderson, J. C.; Yao, Y.; Tour, J. M.; Shashidhar, R.; Ratna, B. R. *Nat. Mater.* **2005**, *4*, 167−172.
(13) (a) Donhauser, Z. J.; Mantooth, B. A.; Kelly, K. F.; Bumm, L. A.; Monnell, J. D.; Stapleton, J. J.; Price, D. W., Jr.; Rawlett, A. M.; Allara, D. L.; Tour, J. M.; Weiss, P. S. *Science* **2001**, *292*, 2303−2007. (b) Lewis, P. A.; Inman, C. E.; Maya, F.; Tour, J. M.; Hutchison, J. E.; Weiss, P. S. *J. Am. Chem. Soc.* **2005**, *127*, 17421−17426.
(14) (a) Bumm, L. A.; Arnold, J. J.; Dunbar, T. D.; Allara, D. L.; Weiss, P. S. *J. Phys. Chem. B* **1999**, *103*, 8122. (b) Moth-Poulsen, K.; Patrone, L.; Stuhr-Hansen, N.; Christensen, J. B.; Bourgoin, J. P.; Bjornholm, T. *Nano Lett.* **2005**, *5*, 783−785. (c) Blum, A. S.; Ren, T.; Parrish, D. A.; Trammell, S. A.; Moore, M. H.; Kushmerick, J. G.; Xu, G.-L.; Deschamps, J. R.; Pollack, S. K.; Shashidar, R. *J. Am. Chem. Soc.* **2005**, *127*, 10010−10011. (d) Monnell, J. D.; Stapleton, J. J.; Dirk, S. M.; Reinerth, W. A.; Tour, J. M.; Allara, D. L.; Weiss, P. S. *J. Phys. Chem. B* **2005**, *109*, 20343−20349.
(15) Xiaoyin, X.; Xu, B.; Tao, N. J. *Nano Lett.* **2004**, *4*, 267−271.
(16) Seferos, D. S.; Trammell, S. A.; Bazan, G. C.; Kushmerick, J. G. *Proc. Natl. Acad. Sci. U.S.A.* **2005**, *102*, 8821−8825.
(17) (a) Bazan, G. C.; Oldham, W. J.; Lachicotte, R. J.; Tretiak, S.; Chernyak, V.; Mukamel, S. *J. Am. Chem. Soc.* **1998**, *120*, 9188−9204. (b) Zyss, J.; Ledoux, I.; Volkov, S.; Chernyak, V.; Mukamel, S.; Bartholomew, G. P.; Bazan, G. C. *J. Am. Chem. Soc.* **2000**, *122*, 11956−11962. (c) Wang, S.; Bazan, G. C.; Tretiak, S.; Mukamel, S. *J. Am. Chem. Soc.* **2000**, *122*, 1289−1297. (d) Bartholomew, G. P.; Bazan, G. C. *Acc. Chem. Res.* **2001**, *34*, 30−39.
(18) Seferos, D. S.; Banach, D. A.; Alcantar, N. A.; Israelachvili, J. N.; Bazan, G. C. *J. Org. Chem.* **2004**, *69*, 1110−1119.
(19) Maercker, A. *Org. React.* **1965**, *14*, 270−490.
(20) Heck, R. F. *Org. React.* **1982**, *27*, 345−390.
(21) (a) Tiecco, M.; Tingoli, M.; Testaferri, D. C.; Maiolo, F. *Synthesis* **1982**, 478−480. (b) Testaferri, L.; Tiecco, M.; Tingoli, M.; Chianelli, D.; Montanucci, M. *Synthesis* **1983**, 751−755.
(22) Lavallee, D. K.; Xu, Z.; Pina, R. *J. Org. Chem.* **1993**, *58*, 6000−6008.

Scheme 1. Synthetic Route to 1,4-Bis[4′-(thioacetylmethyl)styryl]benzene (**3**)

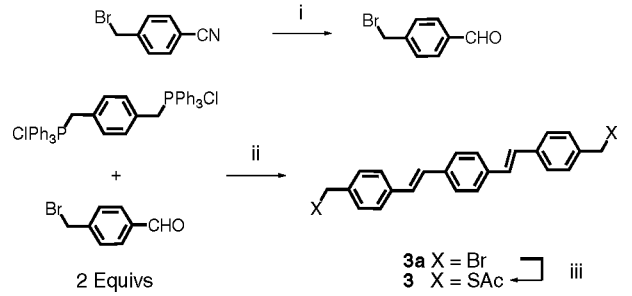

[a] Reagents and conditions: (i) *i*-Bu_2AlH, dichloromethane; (ii) LiOEt, EtOH; (iii) KSAc, DMF.

Scheme 2. Synthetic Route to 1,4-Bis[4′-ethyl(thioacetyl)styryl]benzene (**4**)

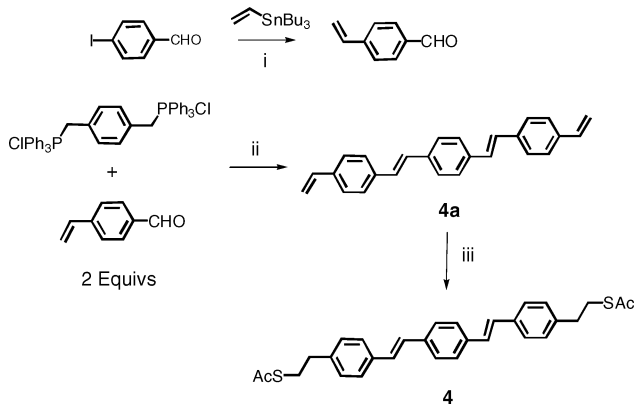

[a] Reagent and conditions: (i) $Pd(PPh_3)_4$, toluene; (ii) LiOEt, EtOH; (iii) AcSH, AIBN, toluene.

phosphonium chloride)benzene is used to form 1,4-bis[4′-(bromomethyl)styryl]benzene (**3a**) in 50% yield. Finally, nucleophilic displacement of the benzylic bromides with potassium thioacetate affords **3** in 61% yield. A key advantage of this route is that the surface-active thioacetate moieties are installed intact in the last step, which eliminates the need for a transprotection step and shortens the overall synthetic pathway. In this case, however, a thermal isomerization step was required to produce the desired *E*,*E* isomer.

Synthetic entry into **4** begins with the conversion of 4-iodobenzaldehyde to 4-vinylbenzaldehyde by treatment with vinyltributylstannane under Stille-type conditions (Scheme 2).[23] Next, a 2-fold Wittig-type reaction of 4-vinylbenzaldehyde and 1,4-bis(methyltriphenylphosphonium chloride)benzene is used to provide 1,4-bis(4′-vinylstyryl)benzene (**4a**) in 63% yield. Finally, treatment of **4a** with thioacetic acid in the presence of the radical initiator AIBN affords the desired product **4** in 47% yield. In this example, the thermal conditions of the final reaction concurrently isomerize the product and only the desired *E*,*E* isomer was recovered. Olefin stereochemistry was confirmed by ^1H and ^{13}C NMR spectroscopy.

Monolayer Characterization. Self-assembled monolayers of **1**−**4** were prepared by immersing cleaned gold electrodes into 0.3 mM solutions of the compounds in ethanol and dichloromethane (1:2) for 14 h. After thorough rinsing in dichloromethane, ethanol, and water, the blocking characteristics of the films were examined by cyclic voltammetry (C-V) measurements in ferricyanide solution[24] (see Figure S1 in the Supporting Information). Comparison of measurements using electrodes modified with **1**, **2**, and **3** with an unfunctionalized electrode indicates that these compounds significantly slow the rate of heterogeneous electron transfer by forming a blocking film. However, the electrode that was functionalized with **4** showed a response similar to that of the unfunctionalized electrode. The added flexibility induced by the incorporation of two ethylene units into the rigid π-backbone of **4** could allow the molecule to adopt a geometry where both thiols are bound to the gold surface with the molecule lying flat on the surface. Although the exact orientations of the molecules cannot be determined by electrochemical experiments, the poor blocking quality suggests that vertical, closely packed monolayers are not obtained with **4**. We conclude that in the case of **4** a poor quality film significantly limits the number of techniques that can be used to measure the conductivity across this type of structure because most measurements require a well-formed film.[1]

STM Apparent Height Measurements. To circumvent the difficulties presented by the poorly defined monolayers obtained with **4**, two-component SAMs were formed by inserting OPVs **1**−**4** into an undecanethiol on a Au(111) matrix monolayer. Under these conditions, the conjugated molecules are inserted into the matrix film at step edges and domain boundaries where it has been demonstrated that they are electronically isolated and exist in an upright fashion due to the rigidity of the supporting monolayer matrix.[25] The surfaces were imaged by STM measurements with the tip biased under constant current feedback control. Inserted molecules appear as bright spots in the image due to differences in both their physical height and their electronic properties relative to the alkane monolayer (Figure 2). Although the apparent height measured from these STM images represents a convolution of both physical and electronic properties, this parameter can be used to calculate the tunneling decay constant relative to the known physical height differences of the two components and the well-studied electronic properties of the matrix film.

To enable quantitative analysis of the STM images, a model is needed that relates the apparent height measured by STM to the molecular conductance. For an STM tip probing a surface-bound molecule, the tunneling electrons transit two distinct regions: the gap between the tip and the molecule and the molecular backbone. Following the formalism of Weiss and coworkers,[14a,d] this process can be represented by a two-layer tunnel junction model (Figure 3) where the transconductances (G) across each layer are

$$G_{gap} = A \exp(-\alpha d_{gap}) \quad (1)$$

and

$$G_{mol} = B \exp(-\beta h_{mol}) \quad (2)$$

where α and β are the tunneling decay constants, A and B are the contact conductances, and d_{gap} and h_{mol} are the thicknesses of the gap and the molecule, respectively. The total trans-

(23) McKean, D. R.; Parrinello, G.; Renaldo, A. F.; Stille, J. K. *J. Org. Chem.* **1987**, *52*, 422−424.

(24) Porter, M. D.; Bright, T. B.; Allara, D. L.; Chidsey, C. E. D. *J. Am. Chem. Soc.* **1987**, *109*, 3559−3568.

(25) Cygan, M. T.; Dunbar, T. D.; Arnold, J. J.; Bumm, L. A.; Shedlock, N. F.; Burgin, T. P.; Jones, L., II; Allara, D. L.; Tour, J. M.; Weiss, P. S. *J. Am. Chem. Soc.* **1998**, *120*, 2721−2732.

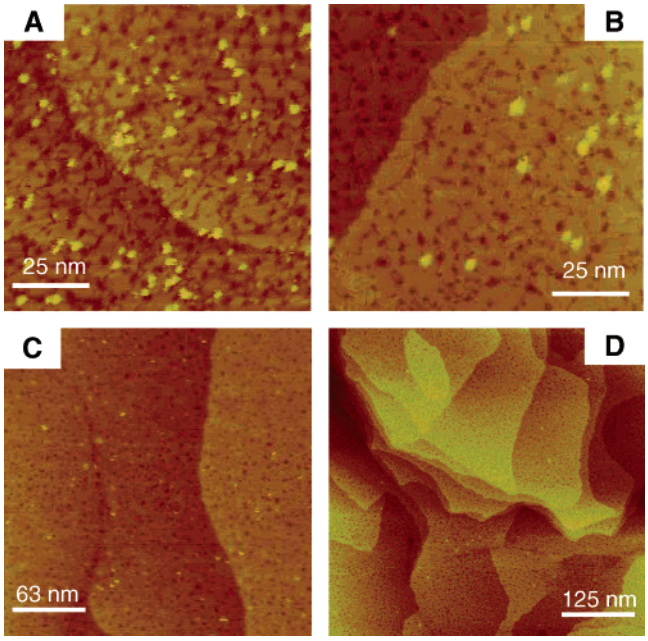

Figure 2. Constant current STM images (I = 2.5 pA, V = 1 V) of molecules **1**−**4** on Au(111) inserted into an undecanethiol SAM. Inserted molecules **1** (A), **3** (B), **4** (C), and **2** (D) appear as bright spots in the images.

conductance of either the inserted molecules or the matrix is the product of the conductances of these two layers, $G_{total} = G_{gap}G_{mol}$. Images are acquired in constant current mode; therefore, G_{total} is constant over the entire image regardless of which feature is probed so that

$$G_{gap1}G_{mol1} = G_{gap2}G_{mol2} \quad (3)$$

for a given image. By making the simplifying assumptions that the tunneling properties of the gap are independent of the molecular fragment ($\alpha_1 \approx \alpha_2$, $A_1 \approx A_2$) and that the contact conductance of the Au−S attachment chemistry is the same for all molecules ($B_1 \approx B_2$), eq 3 can be simplified and solved for the tunneling decay constant of the inserted molecule:

$$\beta_{OPV} = [\beta_{C11}h_{C11} - \alpha(\Delta STM - \Delta h)]/h_{OPV} \quad (4)$$

where ΔSTM is the measured apparent height difference, Δh is the calculated physical height difference, and OPV and C11 denote the inserted and matrix molecules, respectively.[26] The decay constant for alkane thiols on gold such as C11 has been determined both electrochemically[27] and by STM measurements[14a] and serves as a reference for evaluating the conductivity of the inserted OPV molecules.

The apparent height differences in the STM images therefore provide a measure of β, the tunneling decay constant of the inserted molecules (eq 4). The apparent heights measured and the standard deviation from 100 insertion events for each molecule are 10.0 ± 1.0, 8.2 ± 1.2, and 5.1 ± 1.5 Å, corresponding to β values of 0.40 ± 0.12, 0.73 ± 0.13, and 1.24 ± 0.14 Å^{-1}, for **1**, **3**, and **4**, respectively (Table 1). These data indicate the expected trend for molecular conductivity, **1** > **3** > **4**, and that a significant drop in the tunneling efficiency occurs as aliphatic spacer units are inserted between the metal surface and the conjugated molecular fragment, in good agreement with a recent report.[14b] It is significant that the β values calculated for the OPV molecules in this study generally gave much better electronic transparency than those previously observed for other conjugated structures based on the oligo(phenyleneethynylene) structure, which (measured in the same manner) provided a β value of approximately 1 Å^{-1} [14b,c] and highlights the efficient charge transport that characterizes OPV-type structures.

A surprising consequence of the STM imaging is the inconsistency between the calculated tunneling decay constant for **1** and **2** and our previous molecular conductivity measurements using the cross-wire technique that demonstrate nearly identical conductivities for these two molecules.[16] Although compound **1** showed the highest electron transparency, the inserted compound **2** gave an apparent height of only 3.9 ± 2.2 Å, corresponding to β = 1.16 ± 0.25 Å^{-1}. On the basis of our previous conductivity measurements for monolayer samples, we anticipated that **2** would have a tunneling decay constant similar to that of **1**. Instead, compound **2** has a tunneling decay constant that most closely resembles that of **4**, a compound with a total of four methylene spacer moieties.

Molecular Conductivity Measurements. Although several techniques are available to measure the charge-transport properties of molecular junctions, most require the molecules to be

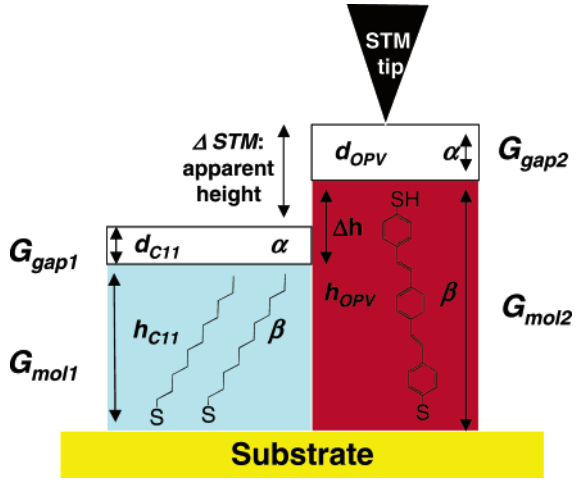

Figure 3. Schematic illustration of the two-layer tunnel junction model used to represent the two-component SAMs. Here, h and d are the layer thicknesses, α and β are the tunneling decay constants, and G_{gap} and G_{mol} are the conductances of the gap and molecule, respectively. ΔSTM is the measured apparent height difference, and Δh is the geometric height difference of the different components of the film.

Table 1. STM Apparent Height and Conductivity Data

compound[a]	length (Å)[b]	apparent height (Å)[c]	β (Å^{-1})[d]	conductivity G (nS)[e]	relative conductivity C-AFM[f]	relative conductivity x-wire[g]
1	19.3	10.0 ± 1.0	0.40 ± 0.12	15.8 ± 6.9	29 ± 13	29 ± 11
2	19.9	3.9 ± 2.2	1.16 ± 0.25	13.6 ± 5.7	25 ± 10	26 ± 13
3	20.8	8.2 ± 1.2	0.73 ± 0.13	5.4 ± 2.5	10 ± 4	
4	24.0	5.1 ± 1.5	1.24 ± 0.14	0.55 ± 0.40	1 ± 0.7	

[a] Structures of the compounds are shown in Figure 1. [b] The sulfur−sulfur distance of the compounds. [c] Measured above the height of the undecane thiol film. [d] Calculated using eq 4. [e] Determined from the slope of the linear low-bias region of the I−V characteristics measured by C-AFM. [f] Conductivity values normalized to molecule **4**. [g] Determined from cross-wire measurements and packing density calculations (ref 16), normalized to the relative conductance of **1** as measured by C-AFM.

(26) Literature values of α = 2.3 and β_{C11} = 1.2 Å^{-1} were used for the calculation (ref 14). The thickness of the C11 monolayer is assumed to be 12.5 Å, corresponding to a tilt angle of 30°.

(27) Weber, K.; Hockett, L.; Creager, S. *J. Phys. Chem. B* **1997**, *101*, 8286−8291.

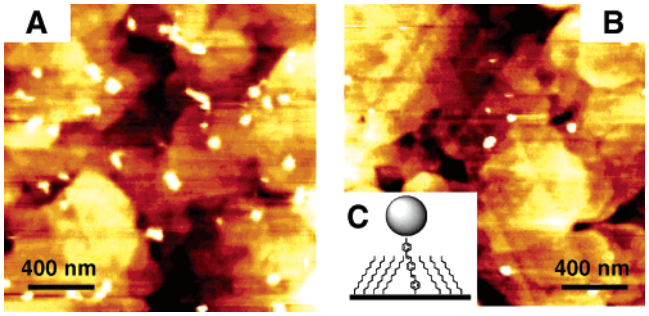

Figure 4. AFM images (contact mode) of inserted molecules **2** (A) and **4** (B) with attached gold colloids. Inset (C) shows a cartoon of the proposed structure. Topographic images of inserted molecules **1** and **3** with attached colloids were similar.

structurally robust and in an upright orientation relative to the surface.[1] Because of the uncertainties in monolayers prepared from **4**, a technique was chosen that directly measures the conductivity of inserted molecules in a matrix film through the attachment of gold colloids that are subsequently contacted and measured with a C-AFM tip. There are two primary advantages to this method. First, the molecules are all forced into a similar upright orientation due to the nature of the insertion process. Second, an analogous molecular geometry to the STM imaging experiments is achieved, which should allow for the best comparison of the two techniques. Lindsay and co-workers have previously demonstrated that this technique provides a reproducible measure of single-molecule conductivity for saturated alkanedithiols[28] and for similar conjugated oligo(phenylene-ethynylene) dithiols.[29]

Inserted molecules **1**−**4** were functionalized with gold colloids through attachment to their unbound protruding thiol functionality by soaking the two-component SAMs in a solution of 5 nm diameter colloids for 1 h, followed by rinsing with water. After the attachment step, the inserted molecules were visualized from AFM imaging by the appearance of their attached colloids, as shown in Figure 4. Images could be obtained in either noncontact (tapping mode) or contact mode with a metal-coated tip. The colloids were stable toward multiple scanning passes, indicating that they are mechanically robust and that the scanning probe tip does not significantly perturb the overall structure.

A closed-loop x−y piezo scanner was used to position the conductive tip directly over the gold colloids, and the current−voltage ($I-V$) characteristics were directly measured. $I-V$ traces recorded on 10−20 individually addressed colloids per sample generally showed a symmetric $I-V$ behavior that was stable to multiple scans in the ±1 V potential range (Figure 5). These $I-V$ measurements demonstrate the same trend in conductivity that was observed in the STM images, **1** > **3** > **4**. The conductivities of the molecules, calculated from the slope of the linear low-bias regime, are 15.8 ± 6.9, 13.6 ± 5.7, 5.4 ± 2.5, and 0.55 ± 0.40 nS for **1**, **2**, **3**, and **4**, respectively (Table 1). The consequence of including a methylene spacer at each end of the OPV structure results in a 3-fold decrease in conductivity. Good agreement is found with a previous report that compares the conductivity of 1,4-benzenedithiol with 1,4-

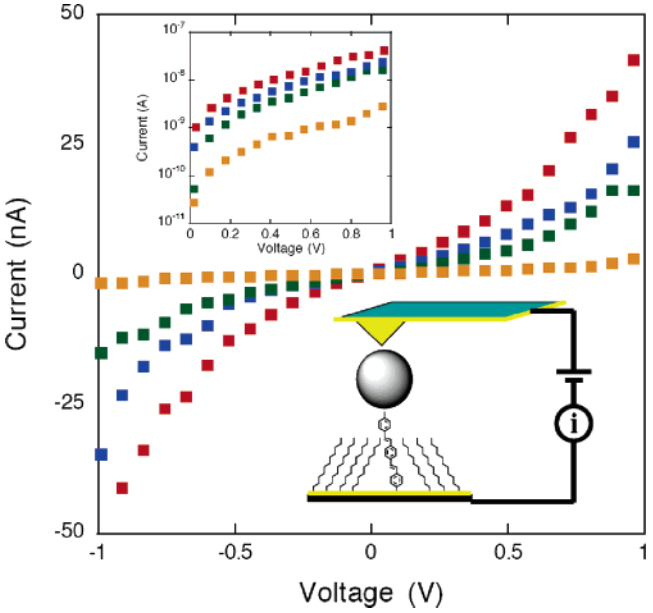

Figure 5. Single-molecule conductivity (current vs voltage) measured on Au−molecule−Au colloid junctions formed from inserted molecules **1** (red), **2** (blue), **3** (green), and **4** (orange), averaged from 10 to 20 individually contacted colloids per sample. Upper inset shows the same data plotted on a semilog scale, and the lower inset shows a cartoon illustration of the measurement.

benzenedimethanethiol and reveals a similar reduction in conductivity that is imposed by the methylene spacer units.[15] Additionally, when extending the study to **4**, which has two methylene units per thiol attachment, a nearly 30-fold drop in conductivity relative to the parent compound **1** is observed (Table 1). This last result highlights how further spacing of the thiol functionality from the OPV core disrupts efficient charge transport.

A notable observation is the high conductivity demonstrated in the $I-V$ characteristics of **2**. Although STM imaging suggested that this structure would have charge transport properties similar to **4**, molecular conductivity measurements by using C-AFM demonstrate that this molecular fragment is more similar to **1**, which is in good agreement with our previous report that demonstrates that these two structures have similar charge-transport characteristics (Table 1). One possible explanation for the discrepancy could be related to the difference in the contacts that the molecules experience in the two measurements. Specifically, in the AFM experiment, both thiol functionalities are chemically bound to a gold surface, whereas in the STM measurements, only one of the thiol end groups is attached.

Electronic Structure Calculations. To gain insight into how the different measurement techniques might influence charge-transport properties, electronic structure calculations were performed on **1** and **2** bound to one and two Au contacts within the density functional theory approximation.[30] In these calculations, one Au contact is representative of the electronic structure probed in the STM measurement, and two Au contacts are used to simulate the electronic structure probed in the C-AFM measurements. The density functional theory calculations were performed using the B3LYP functional[31] coupled with the

(28) Cui, X. D.; Primak, A.; Zarate, X.; Tomfohr, J.; Sankey, O. F.; Moore, A. L.; Moore, T. A.; Gust, D.; Nagahara, L. A.; Lindsay, S. M. *J. Phys. Chem. B* **2002**, *106*, 8609−8614.
(29) Rawlett, A. M.; Hobson, T. J.; Nagahara, L. A.; Tsui, R. K.; Ramachandran, G. K.; Lindsay, S. M. *Appl. Phys. Lett.* **2002**, *81*, 3043−3045.
(30) Frisch, M. J. et al. *Gaussian 03*, revision C.02; Gaussian, Inc.: Wallingford, CT, 2004.
(31) Becke, A. D. *J. Chem. Phys.* **1998**, *98*, 5648−5652.

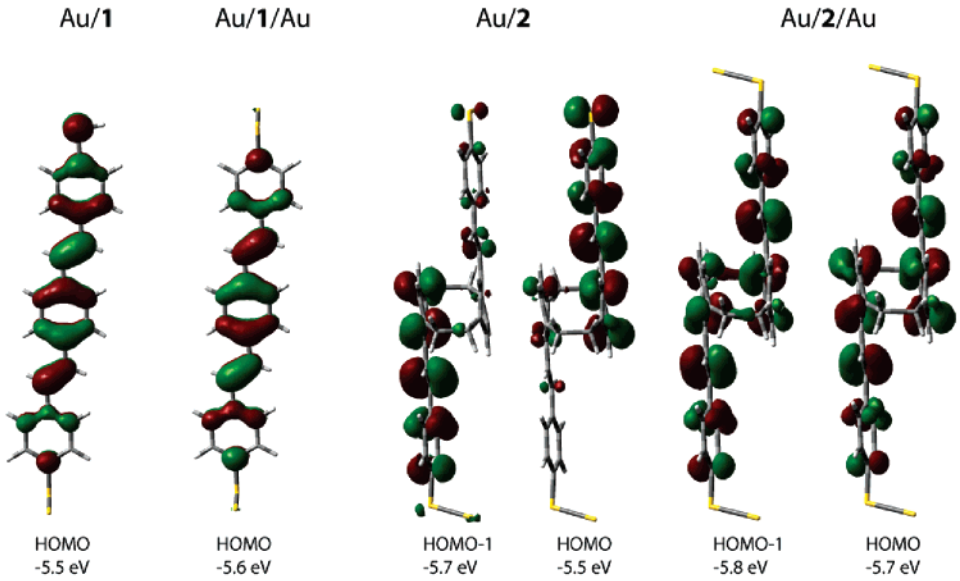

Figure 6. Charge density plots of the highest-occupied molecular orbitals for **1** and **2** attached to one and two gold atoms (Au/**1**, Au/**1**/Au, Au/**2**, and Au/**2**/Au, respectively).

LANL2DZ basis set[32] for all atoms. Single Au atoms attached to the thiol groups were used to represent the molecule electrode interaction. Although single Au atoms are clearly not equivalent to an extended gold surface, previous studies have demonstrated the utility of such calculations to predict likely conductance channels.[33] Specifically, molecular orbitals that span the entire length of the molecule and are energetically similar to the electrode Fermi level are considered good conductance channels. On the basis of these criteria, we identify the highest occupied molecular orbital (HOMO) of **1** and the HOMO and HOMO-1 orbitals of **2** to be the most likely conduction channels for the two systems, respectively (Figure 6).[16]

In the case of **1**, calculations reveal similar topologies for the HOMO, whether the molecule is bound to one (Au/**1**) or two (Au/**1**/Au) gold atoms. The HOMO is delocalized across the entire molecular framework for both Au/**1** and Au/**1**/Au, and the orbitals lie close in energy to the Au Fermi level ($E_f = -5.3$ eV)[34] (Figure 6). Close inspection reveals that a minor asymmetry is apparent for Au/**1**. Different results are observed when the analogous calculation was performed on **2**. Although the HOMO and HOMO-1 structure with two Au atoms (Au/**2**/Au, Figure 6) has a fully delocalized electronic structure that extends across the length of the molecule and demonstrates the through-space mixing of states across the central [2.2]paracyclophane core, the HOMO and HOMO-1 of the singly bound Au/**2** molecule lacks these features. Specifically, the spatial degeneracy of the HOMO and HOMO-1 orbitals is lifted by the single Au contact and the charge density is localized on the upper and lower π-conjugated fragment, respectively. Such localization of the formerly continuous conduction channel highlights why the singly bound molecule has such drastically different charge-transport characteristics when compared to the doubly bound species. In the STM measurements, the tunneling charge carrier has a farther distance to travel (experiences a wider tunnel barrier) before reaching the delocalized molecular orbital.

Summary Discussion and Conclusion

We have provided a comparison of two commonly employed molecular conductance measurement techniques. Both agreement and disconnect were found between the tunneling decay constants obtained by barrier height calculations using STM imaging and molecular conductivity measured by C-AFM on inserted molecules (Table 1). From the molecular perspective, the two techniques differ by the number of chemical (gold) contacts that are made to molecules under investigation. A single gold surface contacts the inserted molecules in STM measurements, and in the case of C-AFM, a top gold colloid is chemically attached to create a more symmetric metal−molecule−colloid junction. Whether the different types of contacts inherent to the measurements result in different measured charge-transport characteristics, and thereby correlate with each other, thus depends on the electronic structure of the bridging molecule.

In the series of related OPV molecules that incorporates increasing methylene functionalities (**1**, **3**, and **4**), STM imaging and conductivity measurements are well matched (Table 1). For these compounds, the HOMO distributions are nearly identical when one or two of the terminal thiols are bound to gold, as determined by DFT modeling. However, the more topologically complex structure **2** is more greatly perturbed under the two different contact geometries. As demonstrated by DFT calculations, the Au/**2** geometry results in localization of HOMO and HOMO-1, when compared to the symmetric Au/**2**/Au situation. In this case, the general electronic distribution of the molecular bridge is considerably different for the two measurement techniques. With this consideration, the apparent disconnect between the measured barrier height and the measured conductance is understood.

The contact geometry in C-AFM measurements is similar to the geometry contacted in previous cross-wire junction measure-

(32) Hay, P. J.; Wadt, W. R. *J. Chem. Phys.* **1985**, *82*, 299−310.
(33) (a) Derosa, P. A.; Seminario, J. M. *J. Phys. Chem. B* **2001**, *105*, 471−481. (b) Heurich, J.; Cuevas, J. C.; Wenzel, W.; Schon, G. *Phys. Rev. Lett.* **2002**, *88*, 256803.
(34) Lide, D. R. *CRC Handbook of Chemistry and Physics*; CRC: Boca Raton, FL, 1998.

ments. This point is highlighted by the excellent experimental agreement that we have observed between the relative conductance of **1** and **2** in the C-AFM-based measurements presented here and previous cross-wire conductivity measurements (Table 1). The results obtained in these independent examinations demonstrate that conductivity of **1** and **2** are the same, within experimental error, when contacted via a symmetric metal−molecule−metal junction geometry. This similar charge-transport is a consequence of the strong through-space π-coupling that is experienced when π-conjugated molecular structures are brought in contact via the [2.2]paracyclophane arrangement.[17]

As a supplement to these metal−molecule−metal junction measurements, probing molecule **2** in the STM geometry yields further information about the electronic properties of this molecule. We speculate that the decreased conductance of **2** that results from a single contact is related to another feature of the unique through-space delocalization across the central [2.2]paracyclophane core. Namely, molecules closely related to **2** have been shown to be more polarizable when compared to structures similar to **1** which contain only through-bond delocalization.[35]

The observed disconnect between the STM and C-AFM measurements on **2** provides some evidence that STM imaging, taken alone, may not always accurately predict the conductivity of molecules assembled in the metal−molecule−metal junction arrangement. Although this clearly is not true in all cases, it represents one cautionary tale where a difference in the measured molecular charge transport arises solely as a consequence of the test structure. Employing multiple measurement techniques not only serves to test for these types of phenomena but also, as demonstrated in the case of **2**, relates additional information about molecular sensitivity to the local environment. We believe that these observations should provide motivation for using *a combined technique* approach to evaluate molecular charge transport, especially in molecules that contain complex electronic structures.

Experimental Details

General Considerations. The preparation of 4-vinylbenzaldehyde[23] and 4-(bromomethyl)benzaldehyde[22] has been described in the literature, and structures were verified by comparison to those references. Reagents were purchased from Aldrich and used as received. Solvents were the highest grade available, purified by a solvent purification system. Synthetic manipulations were performed on a vacuum/argon manifold under an inert atmosphere using Schlenk techniques. Gold-coated mica substrates (150 nm Au, flame annealed) and 5 nm gold colloids (optical density = 1.1 ± 0.1 at 520 nm, approximately 0.1 g/L) were purchased from SPI Supplies.

1,4-Bis[4′-(bromomethyl)styryl]benzene (3a). In a flame-dried, three-neck flask fitted with a Teflon-coated magnetic stir bar and a needle valve, a rapidly stirring suspension of 1,4-bis[(methyl)triphenylphosphine chloride]benzene (698 mg, 1.00 mmol) and 4-(bromomethyl)-benzaldehyde (408 mg, 2.05 mmol) in anhydrous ethanol (10 mL) was treated dropwise with a 1.0 M solution of lithium ethoxide in ethanol (2.5 mL) at 0 °C. The mixture was allowed to warm to room temperature and was stirred overnight (~14 h). Dilute hydrochloric acid (5 mL) was added, and the precipitates were collected on a glass frit, washed with hexanes, and dried in vacuo to yield 236 mg (50%) of yellow solid. The NMR spectra were consistent with the three isomers of the title compound,[36] which were used in the next step, without isomerization. HRMS-EI: 465.9922 Δ = 2.0 ppm.

1,4-Bis[4′-methyl(thioacetyl)styryl]benzene (3). In a flame-dried, three-neck flask fitted with a Teflon-coated magnetic stir bar and needle valve, **3a** (100 mg, 0.21 mmol) was partially dissolved in anhydrous DMF (10 mL) under an argon atmosphere. Potassium thioacetate (57 mg, 0.50 mmol) was added at once, and the reaction was stirred at room temperature for 75 min and was then heated to 80 °C for 90 min. Upon cooling to room temperature, the solution was diluted with 50 mL of dichloromethane (DCM), washed with water, dried, and concentrated. Purification by chromatography using a 10 cm silica gel column eluting with DCM afforded a mixture of three isomers of the desired product. Thermal isomerization by refluxing in anhydrous toluene with a few crystals of iodine, followed by chromatography, yielded 59 mg (61%) of the *all-E* isomer of the title compound. ^{1}H NMR ($CDCl_3$): 7.51 (s, 4H), 7.46 (d, ^3J = 8.37 Hz, 4H), 7.29 (d, 4H), 7.09 (s, 4H), 4.14 (s, 4H), 2.37 (s, 6H). ^{13}C NMR ($CDCl_3$): 195.4, 137.2, 136.9, 136.6, 129.4, 128.5, 128.2, 127.1, 126.9, 33.5, 30.6. HRMS-EI: 458.1391 Δ = 3.7 ppm.

1,4-Bis[4′-vinylstyryl]benzene (4a). 4-Vinylbenzaldehyde (170 mg, 1.29 mmol) and 1,4-bis[(methyl)triphenylphosphine chloride]benzene (401 mg, 0.58 mmol) were dissolved in anhydrous ethanol, treated with 1.0 M lithium ethoxide in ethanol (1.5 mL), and worked up in the same manner as that described for **3a** to yield 123 mg (63%) of a yellow solid. The NMR spectra were consistent with the three isomers of the title compound,[36] which were used in the next step, without isomerization. HRMS-EI: 334.1716 Δ = 1.8 ppm.

1,4-Bis[4′-ethyl(thioacetyl)styryl]benzene (4). In a flame-dried, three-neck flask fitted with a Teflon-coated magnetic stir bar and a needle valve, **4a** (50 mg, 0.15 mmol), thioacetic acid (32 μL, 0.45 mmol), and AIBN (10 mg) were dissolved in anhydrous toluene. The solution was degassed by three freeze−pump−thaw cycles and was then heated to 90 °C for 24 h. Subsequently, additional AIBN (5 mg) was added and the reaction was continued for an additional 24 h. Upon cooling, the mixture was partitioned between DCM (50 mL) and saturated $NaHCO_3$ (50 mL), extracted with DCM, dried, and concentrated. Purification by chromatography using a 20 cm silica gel column eluting with DCM afforded 34 mg (47%) of the desired product; only the *all-E* isomer was present. ^{1}H NMR ($CDCl_3$): 7.51 (s, 4H), 7.47 (d, ^3J = 8.37 Hz, 4H), 7.23 (d, 4H), 7.10 (s, 4H), 3.14 (t, ^3J = 8.10 Hz, 4H), 2.89 (t, 4H), 2.36 (s, 6H). ^{13}C NMR ($CDCl_3$): 196.0, 139.7, 136.9, 135.9, 129.2, 128.9, 128.4, 128.1, 127.0, 126.9, 35.8, 31.0, 30.6. HRMS-EI: 486.1693 Δ = 1.1 ppm.

C11 Films. A fresh Au/mica Au(111) substrate was cleaned by 10 min exposure to UV−ozone, followed by rinsing with deionized water and ethanol.[37] The cleaned substrate was immersed into 10 mL of an ethanolic solution containing 50 μL of undecanthiol (Aldrich) for 40 min, rinsed with EtOH, and dried with a stream of CO_2.

OPV Insertion. Working in an inert atmosphere glovebox, 1 mg of OPV compound was dissolved in 4 mL of anhydrous THF. Once dissolved, 10 μL of NH_4OH was added, and the solution was agitated for about a minute and passed through a 0.1 μm membrane into a vial containing the C11/Au/mica substrate. After 45 min, the vial was removed, and the substrate was rinsed with THF and EtOH and dried with a stream of CO_2.

Nanoparticle Attachment. The substrate described above was treated with a commercially available solution of 5 nm diameter Au colloids without dilution for 1 h, rinsed with Milli-Q water, and dried with a stream of CO_2.

STM Measurements. Images were obtained in constant current mode (I = 2.5 pA, V = 1.0 V) using a Digital Instruments Multimode scanning probe microscope equipped with a low-current amplifier attachment operated by a Nanoscope IIIa controller. A Pt/Ir tip was used.

(35) Hong, J. W.; Woo, H. Y.; Liu, B.; Bazan, G. C. *J. Am. Chem. Soc.* **2005**, *127*, 7435−7443.
(36) Drefahl, G.; Plötner, G.; Winnefeld, K. *Chem. Ber.* **1961**, *94*, 2002−2010.
(37) Ron, H.; Matlis, S.; Rubinstein, I. *Langmuir* **1998**, *14*, 1116−1121.

AFM Measurements. Images and spectroscopy data were obtained using a PSIA XE-100 scanning probe microscope equipped with an external preamplifier. Contact mode images and current voltage measurements were obtained using a Ti−Pt-coated tip operating at a 2 nN setpoint.

Electronic Structure Calculations. The electronic structure of molecules **1** and **2** coupled to either one or two Au atoms at their thiol end groups was calculated within the density functional theory approximation.[30] The density functional theory calculations were performed by using the B3LYP functional[31] coupled with the LANL2DZ basis set[32] for all atoms. The entire "extended molecule" (molecule plus Au atom(s)) was relaxed to find the final optimized structure before performing the electronic structure calculation.

Acknowledgment. Financial support from the Institute for Collaborative Biotechnology (D.S.S. and G.C.B) and DARPA (J.G.K.) is gratefully acknowledged.

Supporting Information Available: Complete ref 29, cyclic voltammetry data for electrodes modified with molecules **1**−**4**, Cartesian coordinates, and energy of optimized structures. This material is available free of charge via the Internet at http://pubs.acs.org.

JA062898J